Master's Thesis of Landscape Architecture

Continuous observation of vegetation indices, leaf area index (LAI) and fraction of absorbed photosynthetically active radiation (fPAR) using an integrated low-cost near surface sensing system

저렴한 근접 표면 센서를 이용한 식생 지수, 엽면적 지수, 광합성유효복사량의 흡수률 관찰

August, 2017

Graduate School of
Seoul National University

Department of Landscape Architecture and Rural Systems Engineering, Landscape Architecture Major

Kim, Jongmin

Abstract

Monitoring vegetation indices, fraction of absorbed photosynthetically active radiation (fPAR) and leaf area index (LAI) has advanced our understanding of biosphere-atmosphere interactions. Although there are continuous observations for each variable, monitoring vegetation indices, fPAR and LAI simultaneously is still lacking. Recent advances of technology provide unprecedented opportunities to integrate various low-cost sensors as an intelligent near surface observation system for monitoring ecosystem structure and functions. In this study, we developed a Smart Surface Sensing System (4S), which can automatically collect, transfer, process and analyze data, and then publish time series results on public-available website. The system is composed of micro-computers, micro-controllers, multi-spectral spectrometers made from Light Emitting Diode (LED), micro cameras, and Internet module. We did intensive tests and calibrations in the lab. Then, we conducted *in-situ* observations of normalized difference vegetation index (NDVI), enhanced vegetation index (EVI), fraction of absorbed photosynthetically active radiation (fPAR), and leaf area index (LAI) continuously at a rice paddy field during the growing season. NDVI and EVI obtained by 4S showed linear relationships with those from a reference hyperspectrometer ($R^2 = 0.98$; NDVI, $R^2 = 0.96$; EVI). 4S derived fPAR and LAI were comparable to LAI-2200 and destructive measurements in both magnitude and seasonal trajectory. We retrieved vegetation indices, fPAR and LAI independently and continuously and show that after the reproductive stage, fPAR remained constant, whereas LAI and NDVI decreased continuously after their peak because of non-photosynthetic materials such as grain and yellow leaf. In addition, using vegetation index to estimate fPAR has limitation because the spectral reflectance could not capture the diurnal pattern. On the other hand, fPAR changes abruptly depending on the sky conditions and the amount of light transmitted. We believe that 4S will be useful in the expansion of ecological sensing networks across multiple spatial and temporal scales.

Keywords : Leaf area index, Vegetation indices, Fraction of absorbed photosynthetically active radiation, Near surface sensor, Remote sensing

Student Number : 2015-23120

Contents

List of figures

1 Introduction

Monitoring vegetation indices, fraction of absorbed photosynthetically active radiation (fPAR) and leaf area index (LAI) has advanced our understanding of biosphere-atmosphere interactions (Sellers et al., 1997). These three variables explain light interception by canopies (Baldocchi et al., 1984; Myneni et al., 1987; Myneni et al., 1997b), vegetation activity (Tucker, 1979), and carbon and water fluxes (Baldocchi et al., 2002; Leuning et al., 1995; Monteith, 1965; Monteith, 1976). Satellite remote sensing offers maps of these variables in space and time, which help understanding of vegetation response to climate change (Myneni et al., 1997a). In-situ, continuous, concurrent observation of these variables, however, has been rare.

There have been consistent efforts to monitor the individual variables of vegetation indices, fPAR and LAI continuously using near surface sensors. To monitor vegetation indices, Motohka et al. (2009) and Nagai et al. (2014) used a rotating hemispherical spectrometer in rice paddy and deciduous forest. Hilker et al. (2007) integrated a hyperspectrometer, a rotating probe and data logger to measure spectral reflectance at different angles from one tower at a coniferous forest. Ryu et al. (2010a) developed Light Emitting Diode (LED) to measure spectral reflectance and monitor vegetation indices in a savanna, evergreen and deciduous forests (Ryu et al., 2014). To monitor LAI, Ryu et al. (2012) used upward-looking digital cameras in an oak-savanna ecosystem and Yin et al. (2017) developed quantum sensor system to measure light intensity and then estimate LAI. To monitor fPAR, multiple quantum sensors located above and below canopy have been widely used (Inoue et al., 2008; Jenkins et al., 2007). Although there are continuous observations for each variable, monitoring vegetation indices, fPAR and LAI simultaneously is still lacking.

Biophysical variables can be monitored by advanced techniques, such as micro-computer and micro controller, concurrently and continuously. Commercially available micro-computer can save, share and analyze data. (Miorandi et al., 2012). For examples,

Liao et al. (2017) developed a system to monitoring growth of orchids with integrated micro-computer and micro camera and Ferrández-Pastor et al. (2016) used micro-computer connected sensor to measure humidity and temperature and tried to control them constantly. Besides, data processing and sharing can become less time consuming and labor intensive by using the micro-computer with an internet module to monitor field data in real time. (Gressler et al., 2015; Mell and Grance, 2011). The micro-controller changes the signal from the sensor into data that can be saved by the micro-computer and also control the sensor to collect data at a time interval that meets user needs. Previous study confirmed that commercially micro-controllers can convert analog signal to digital number and collect the data continuously with high accuracy (Zhen et al., 2017).

Using micro-computer and micro-controller provides an opportunity to obtain data in multiple plot with high cost efficiency. There have been consistent development to reduce the price of sensor (Bauer et al., 2014; Garrity et al., 2010; Qu et al., 2014; Ryu et al., 2010a; Yin et al., 2017) because near surface sensors, which have a relatively smaller footprint compared to satellite pixel sizes or flux tower footprint, must be installed at various locations to obtain a representative value of the area (Richardson et al., 2013). Although reducing the cost of the sensor is important, it is also necessary to reduce the cost of processing and sharing the data obtained from the sensors. For example, Ryu et al. (2010a) demonstrated that a low cost LED can be used as a spectrometer, however, the price of the existing data logger was more expensive than the sensor. Using micro-computer and micro-controller can solve this problem because they have the potential to substitute existing instruments such as a computer and data logger. Besides, they are high cost efficiency because they have only the minimum functions that are we need.

In this study, we develop a Smart Surface Sensing System (4S), that measures vegetation indices, LAI and fPAR at the same time and then automatically collect, transfer, process data, and then publish time series results on a publicly available website. The system is composed of a micro-computer Raspberry pi, a micro-controller Arduino, multi-spectral spectrometers made from LED, visible cameras, and an Internet module. In this paper, 1)

we describe the novel system and test its performance in the lab, 2) we evaluate the sensor performance at a rice paddy in different locations with manual observation and 3) we observe vegetation indices, fPAR and LAI continuously and simultaneously, and we show the relationship between them. 4) we compare continuously observed data using near surface sensor in field and satellite data with different spatial resolutions.

2 Materials and methods

2.1 Development and calibration of 4S

The system is composed of micro-computers Raspberry pi (Raspberry pi b2 module, Raspberry pi), micro-controllers Arduino (Arduino Nano, Arduino) multi-spectral spectrometers made from LED, visible cameras, and Internet modules. All components are connected and Raspberry pi intelligently controls the automatic data production chain. Raspberry pi collects photos from pi camera and spectral information, which then converts analog signal to digital number from LED spectrometer to the Arduino. Raspberry pi sends the data to a remote server through the File Transfer Protocol (FTP). After collection, we used Javascript to visualize on the web page. (Figure 1).

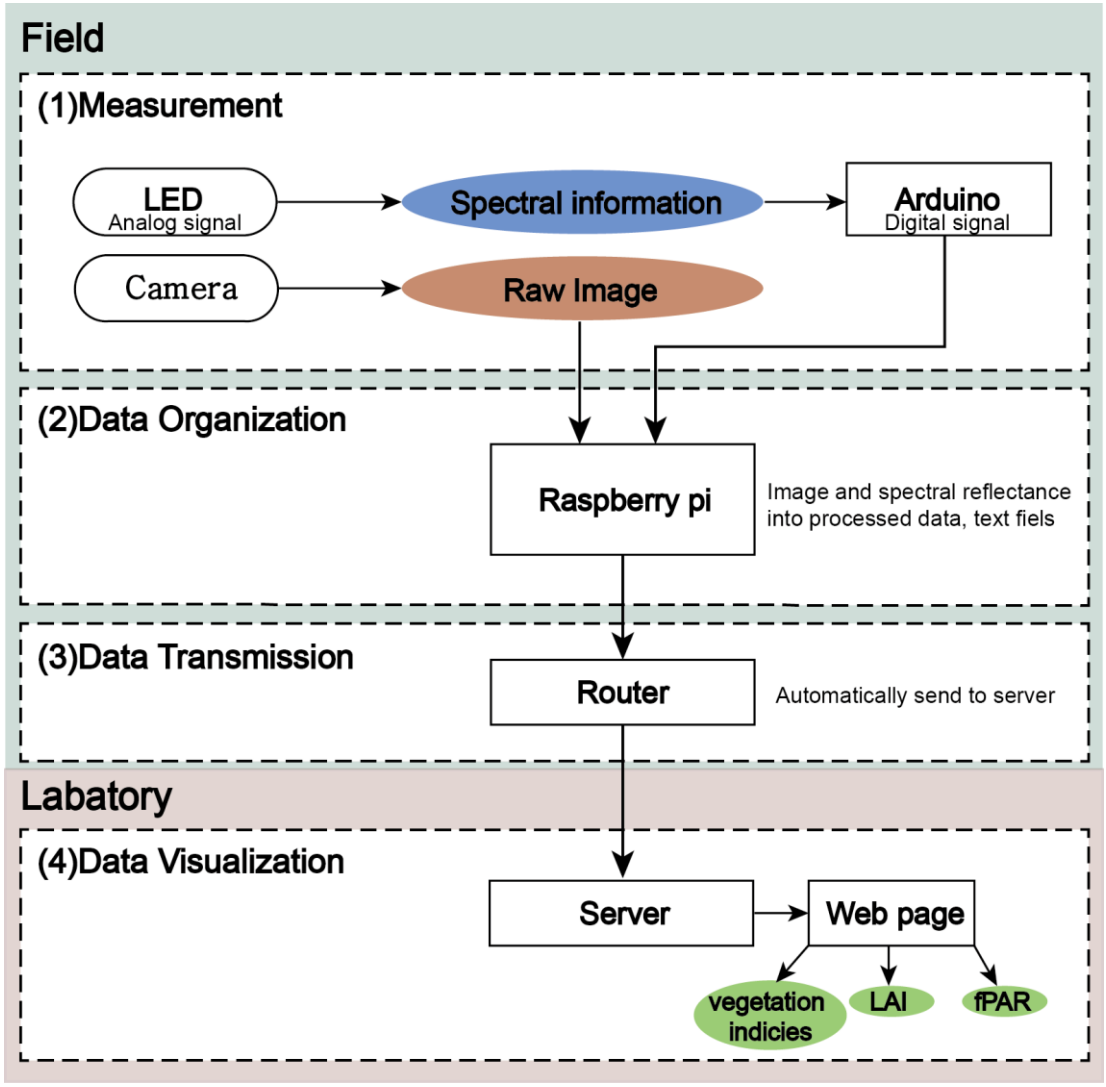

Figure 1. Schematic of smart surface sensing system.

2.2 Testing the 4S LED spectrometer

Although previous studies already used LED to measure light intensity, its production is either discontinued or only available in specific countries, so we tested and selected the led that absorbed light at the required intensity. We tested and chose LED again because that LED was discontinued or produced in specific country. In addition, previous study used a Data logger, such as Campbell products, for converting analog signal to digital number, while we used a low-cost micro controller. We followed the circuit with Ryu et al. (2010a), however, we removed the power supply because the micro controller supports stable electricity to the amplifier (op-amp LTC1060).

Each LED has a different range of wavelengths to be able to sense light, and the intensity to be recognized is different. To select LED, we used Solar cell chamber (Mc Science: K3100 (IPCE)) which emits light over different wavelengths. We saved data absorbed from LED on a wavelength of 300nm to 1100nm with 2nm intervals at 8 seconds. The NIR band was collected at intervals of 50nm. We choose at least three intermediate values before changing the wavelength (Figure 2). We have tried to select an LED similar to the wavelength MODIS recognizes.

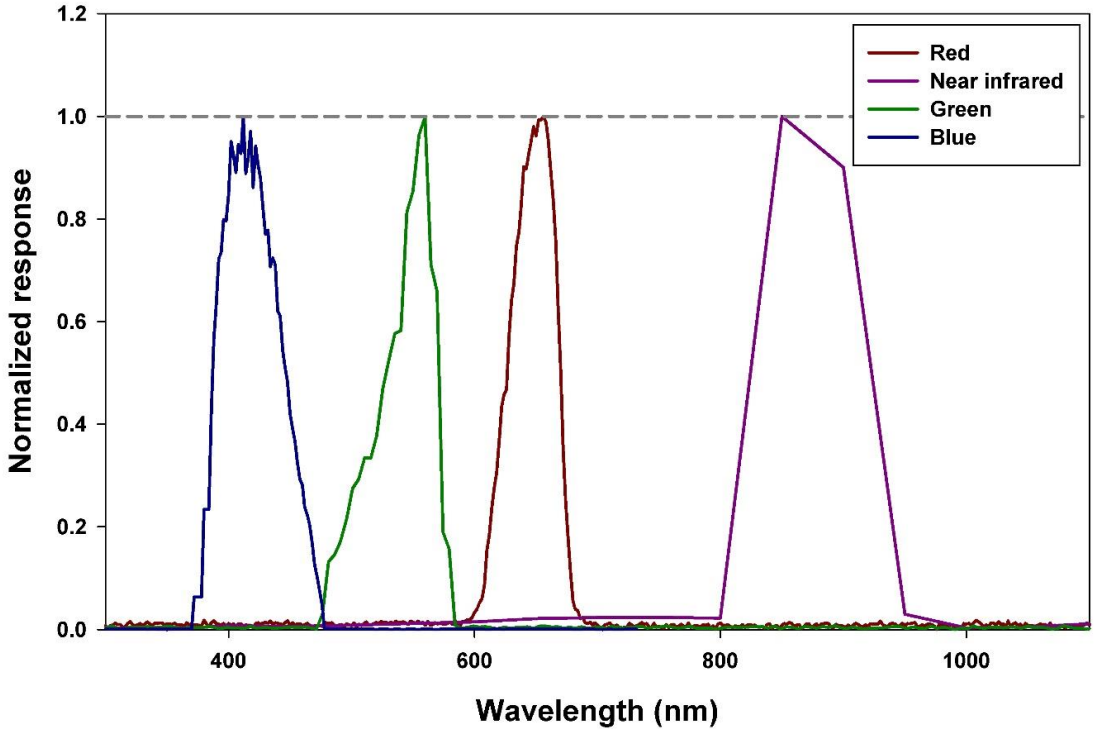

Figure 2) Spectral response of Red (Peak wavelength: 656nm, full-width half maximum (FWHM): 626-670nm, near infrared (Peak wavelength: 850nm, FWHM: 825-925nm), green (Peak wavelength: 560nm, FWHM: 528-570nm) and blue (Peak wavelength: 412nm, FWHM: 387-446nm).

To confirm that LEDs have a linear relationship with the precise instrument in changing light conditions, we compared LEDs to a hyper-spectrometer (ASD hyper-spectrometer., ASD Field spec.) in different solar zenith angles. When the sky condition was clear, PAR irradiance ranging from 28.5 W/m^2 to 496.1 W/m^2, we installed LEDs and hyper-spectrometer horizontality on a rooftop, to avoid shadow effect from any structure. Before testing, we covered LEDs with Teflon (0.5T) to distribute light evenly because each LED head has a different Field of View (FOV). To compare the same wavelengths between LED with ASD hyper-spectrometer, we selected and averaged the wavelengths of the hyper-spectrometer that is the same as the Full Width at Half Maximum (FWHM) of the LEDs (Figure 3).

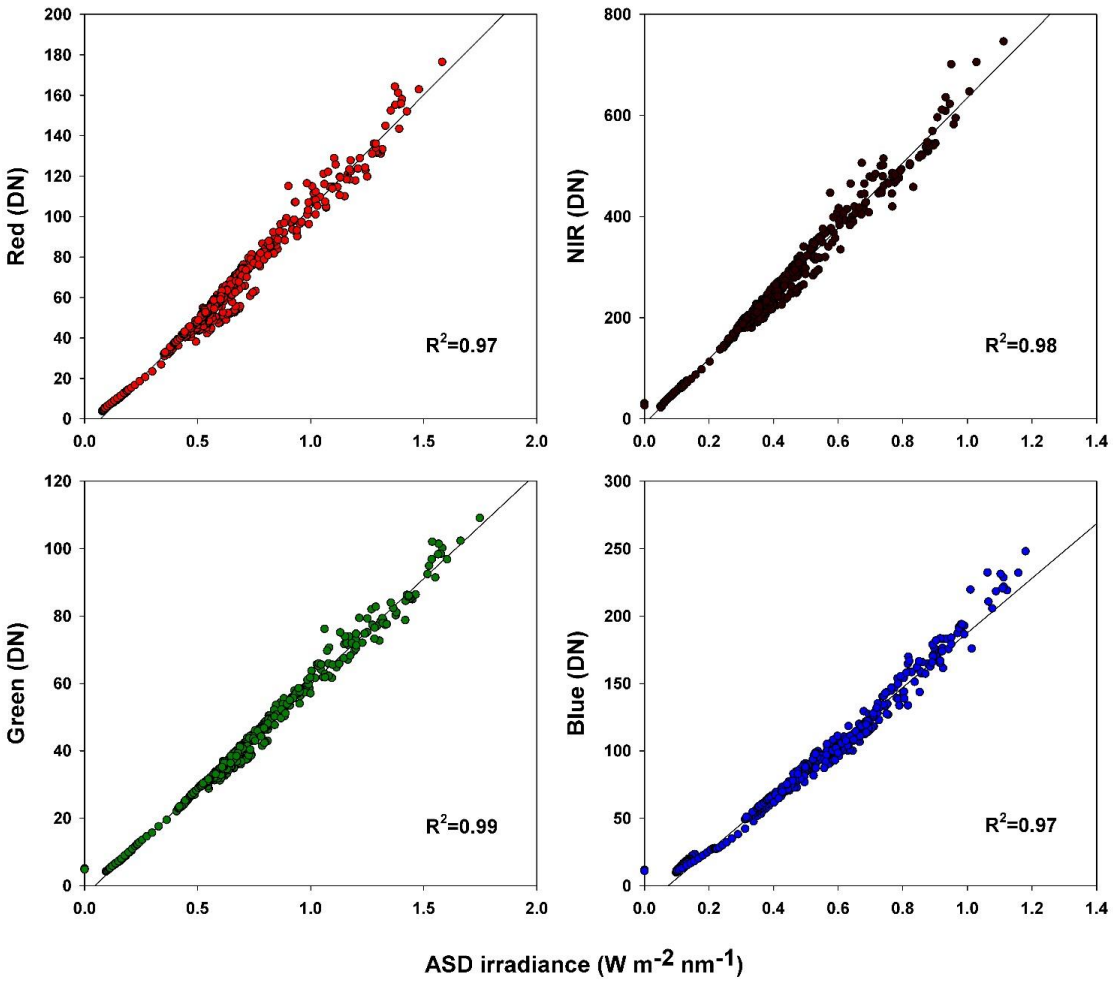

Figure 3) Linearity test of 4S LED-sensor against hyper-spectrometer with changing solar zenith angle (40~70°).

LEDs can measure reflectance as well as PAR. When we did a multi-regression of LEDs (RED, GREEN, BLUE) with the PAR sensor, the pattern and size of LED values are similar to result from the PAR quantum sensor (PQS 1; Kipp & Zonen B.V., Delft, The Netherlands) (Figure 4).

$$4S\ \ PAR = \alpha \times RED\ \ + \ \ \beta \times Green\ \ + \ \ \gamma \times Blue$$

Where α, β and γ are parameters and RED, GREEN, BLUE are bands of LED.

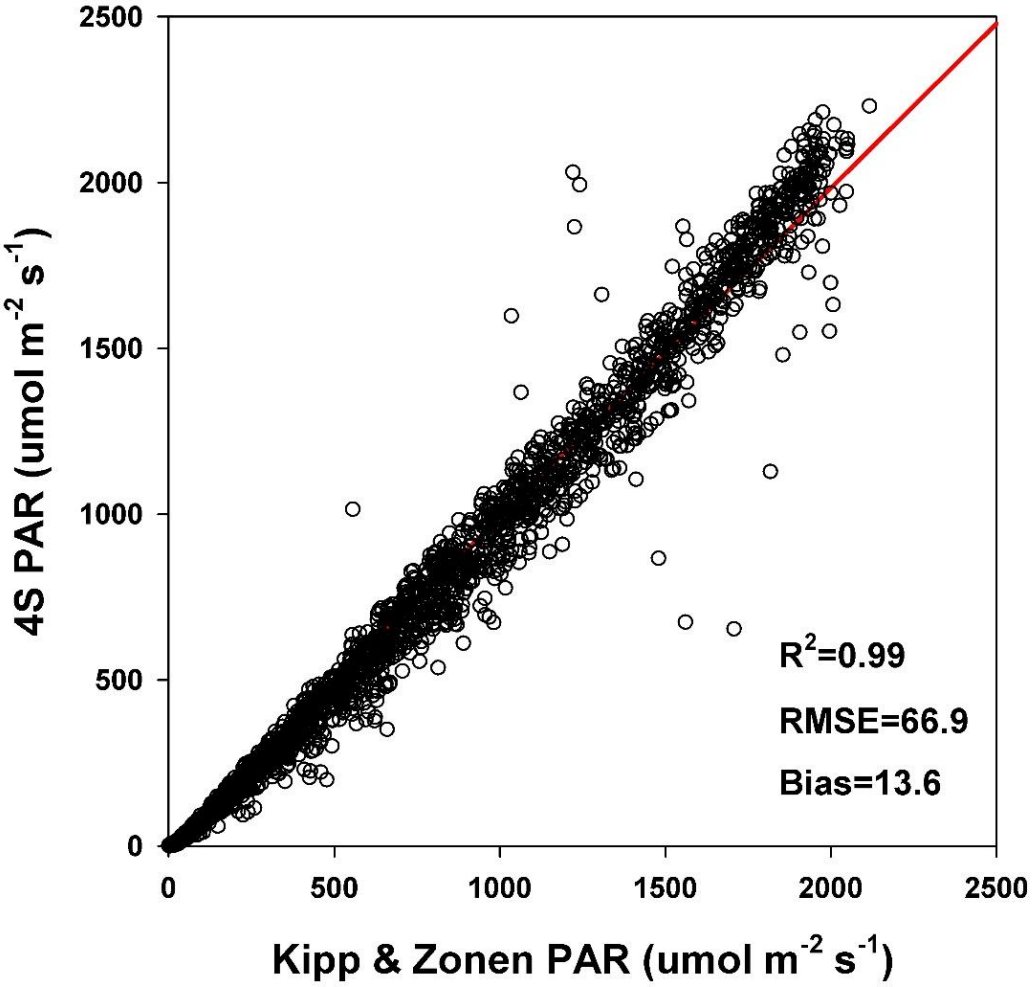

Figure 4) Linearity test of 4S LED-sensor against Kipp & Zonen PAR quantum sensor

2.2.1 Site description

Cheorwon site is an intermittently irrigated rice paddy (38.2017°N, 127.2505°E) located in the central part of the Korean Peninsula. The annual maximum, minimum, mean temperature and precipitation (periods from year 2000 to 2014) are 35.3, -12.3, 10.2°C, and 1,391 mm, respectively (Korean Meteorological Administration weather station data collected 8 km from the study site). The size of the area where the same management takes place is 3528 m^2 (98 m × 36 m) (Figure 5). The cultivated rice species in the field were *O.Sativa.L. cv. Odae1ho*. (Figure 5)

Rice paddy was continuously monitored from May to September 2016. The rice seedling was grown in a greenhouse for 12days and transplanted at a 22 × 10 cm interval on Day of Year (DOY) 120, then, harvested on DOY 248.

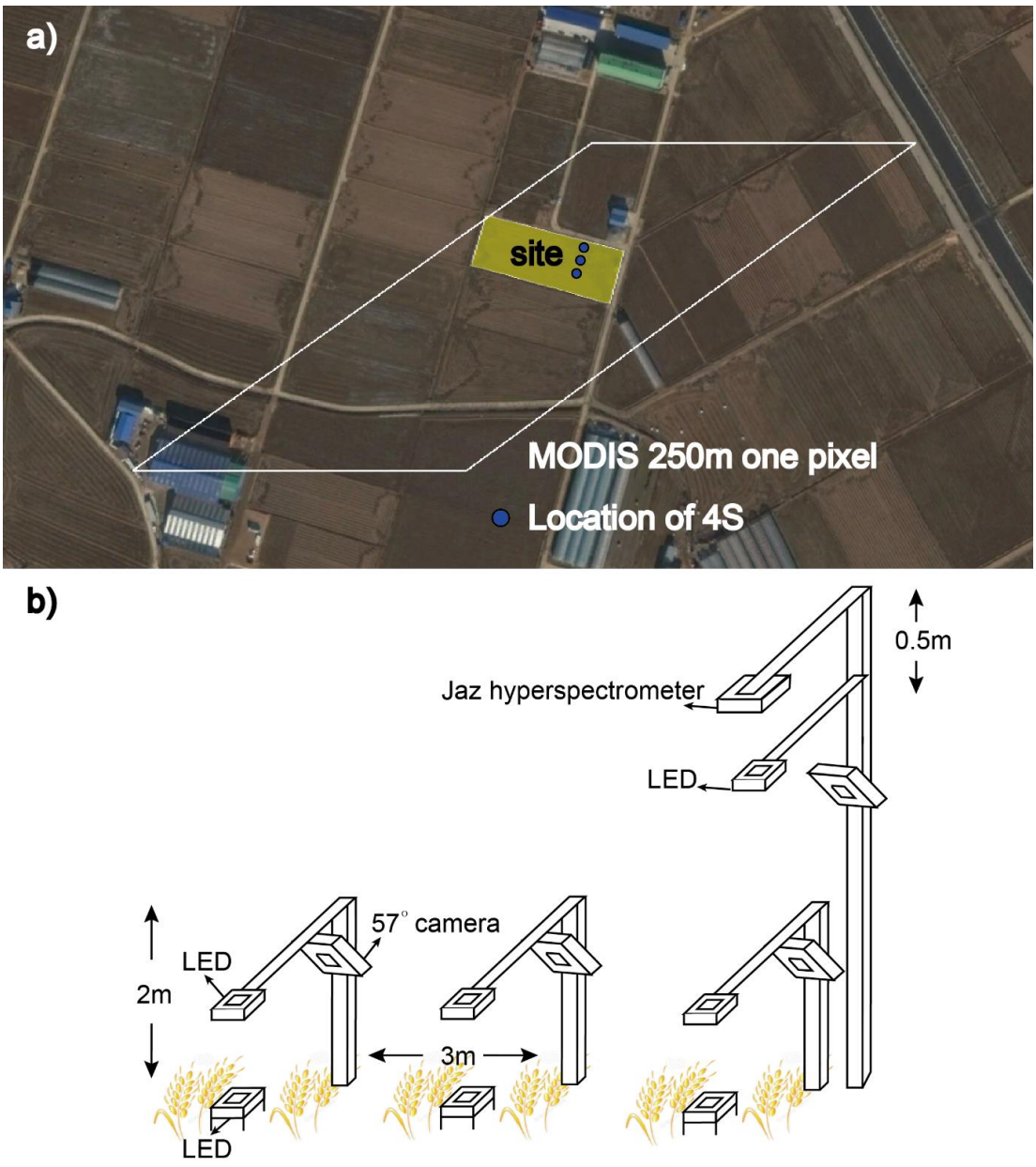

Figure 5) a) Site map. White line pixel boundary of MODIS 250 m. Yellow region is the monitored rice paddy site and blue dot is location of 4S. b) Four 4S are located at 3 m intervals and we installed two LED sensor 2 m above rice and one LED sensor located below the canopy for measuring transmittance.

2.2.2 4S in-situ

We installed LED-sensors on horizontal booms 2m above the ground. One LED sensor was directed to the zenith direction and the other toward the nadir direction (Figure 5b). We cross-calibrated each spectral band between the upward and downward LED-sensors in the lab and field site after harvest. In each plot, the reflectance for each band was calculated and processed to normalized difference vegetation index (NDVI) and enhanced vegetation index (EVI) (Tucker, 1979).

$$\mathrm{NDVI} = \frac{\overline{\rho\mathrm{NIR}} - \overline{\rho\mathrm{RED}}}{\overline{\rho\mathrm{NIR}} + \overline{\rho\mathrm{RED}}}$$

$$\mathrm{EVI} = \frac{G \times (\overline{\rho NIR} - \overline{\rho RED})}{\overline{\rho NIR} + C_1 \times \overline{\rho RED} - C_2 \times \overline{\rho BLUE} + L}$$

Where ρ is spectral reflectance and the overbar indicates the average of the day. The spectral reflectance was calculated by dividing observed data from the downward sensor by the value observed by the upward sensor. G is a gain factor; C_1, C_2 are the coefficients of the aerosol resistance term. L is soil-adjustment factor. We followed MODIS EVI algorithm, where L = 1, C_1 = 6, C_2 =7.5, and G = 2.5 (Huete et al., 2002; Jiang et al., 2008).

PAR was calculated using incoming light from outside of canopy and downward PAR was calculated using the light observed under the canopy. To measure below PAR, we fixed the single LED sensor on styrofoam so that it could float on the water surface. If there is no water, it is flat on the surface. To avoid interfering with harvest, we moved the sensor from ground to deck on DOY 247. We used only the data from 6:30 to 18:30 in order to remove the observed data in the absence of light. fPAR is calculated from the difference in energy entering the canopy and energy leaving the canopy (Begue, 1991). We averaged data over three plot after calculating fPAR from each plot.

$$\text{fPAR} = 1 - \text{transmittance}$$

RGB cameras were installed on the same boom with upward LED to observe the rice paddy at a 57° angle and the time of the photo taken was at 06:00, 12:00 , and 18:00 for each day in each plot. We classified pixels as soil, water or vegetation using red, green and blue channel information extracted from each JPEG image. We modified previous method to distinguish between background pixels with vegetation pixel. Liu and Pattey (2010) made a histogram using greenness value (ExGI) and then set the threshold for distinguish between background and leaf (Figure 6).

$$\text{ExGI} = 2 \times \text{Green} - \text{Red} - \text{Blue}$$

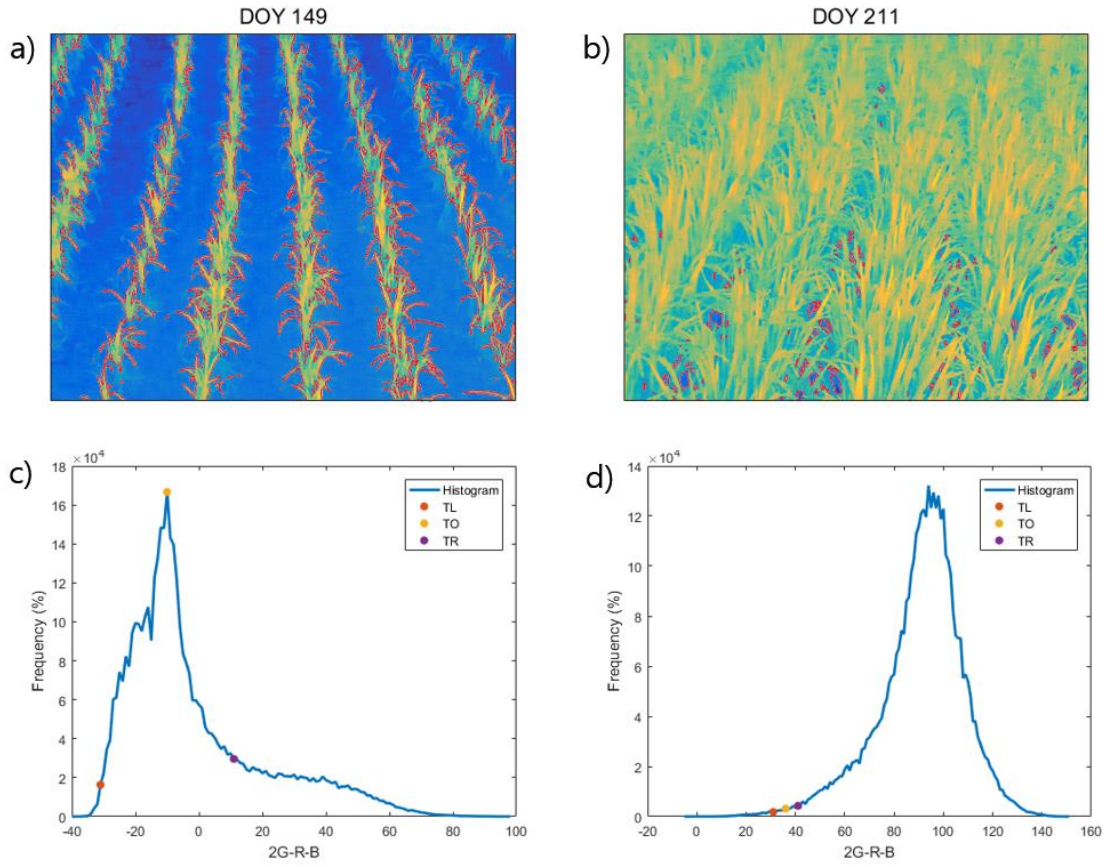

Figure 6) Determination of the threshold for image segmentation. (TL: 0.5% of total number of pixels, TO: maximum frequency, TR: calculate the distance from TL to TO and adds this distance to TO)

Liu and Pattey (2010) set TL, TO and TR to analyze the histogram. The greenness value TO represents that background elements such as water and soil is maximal. TL represents the greenness value below which the proportion of pixels in not more than 0.5% of total number of pixels. TR is the mirror of TL with respect to TO. This method distinguishes well between background pixels with vegetation pixels in the early phenophase, however, when the rice is growing, it does not function well because it is hard to see the background materials after the reproductive stage. To solve this problem, we modified the method to find TO. We set the threshold to find TO less than 25% of total pixels because a peak representing the background occurs below 25% of the total number of pixels. 25% was used as the threshold to distinguish between green leaf and yellow leaf after the reproductive stage.

To estimate LAI, we calculate gap faction by using non-vegetation pixels divided by the number of total pixels.

$$\mathrm{LAI} = \frac{-\log(\overline{gap\ \ fraction})}{k}$$

We calculated *k* by dividing with G-function by degree of cosine 57°. We assumed view zenith angle is 57° and *k* varied to 0.92 because 57° of G-function is 0.5 (Campbell, 1990; Goel and Strebel, 1984). After estimating gap fraction for each image, we selected the highest value and averaged the gap fraction taken on the three plots and then estimated LAI and computed the error with a 95% confidence interval (CI). We averaged gap fraction before calculating LAI to reduce the clumping effect (Ryu et al., 2010b).

One system, consisting of a camera and LEDs, which were 3m apart from each other on the deck. In order to observe the rice paddy from various angles, the observation directions of the three systems were set differently: Along rows, perpendicular to rows, and inclined to rows.

2.2.3 **Reference data collection**

To obtain reference data of the area of the leaves, we collected six rice hills randomly with every two weeks. We scanned and weighed all the leaves of three rice hills in the laboratory. we stick the leaf on the white board and saved the scanned image with 300 dpi and JPEG format when we scanned leaves. At the same time, we separated the grain and measured its weight. To analyze the scanned image, we extracted the blue channel by using Matlab (The MathWorks Inc., Natic, Ma, USA) and distinguish between green leaf with yellow leaf. We set the threshold and tried to separate green and yellow from image. The remaining three hills were dried at 80° C for 48 hours, and we measured the weight to estimate the LAI.

To verify that 4S observes vegetation indices, we installed a 4S and Jaz hyper spectrometer on a 5m high tower. Spectral reflectance data observed by Jaz hyper spectrometer and 4S was saved at a 1 min interval. To compare the daily pattern of NDVI and EVI of Jaz and 4S, we selected and averaged the data at noontime.

To validate 4S fPAR, we visited the site every two weeks and measured fPAR using LAI-2200C Plant Canopy Analyzer (LI-COR, Lincoln, NE, USA). We collected fPAR data at more than 25 points randomly using LAI-2200 in before noontime. We removed any of the five rings if the observations in the below canopy were larger than above measurements. We used Matlab to analyze fPAR data.

2.2.4 Satellite remote sensing data

To highlight the advantages of near surface sensors in rice paddy, we compared the satellite data with difference spatial resolution with observed data using near surface sensor.

We used the MODIS Surface Reflectance products terra and aqua (MOD09GQ and MYD09GQ) with daily interval and 250m resolution. We used only data classified as (a) ideal quality; “MODLAND QA bits” (00) in the MOD09GQ QA descriptions, (b) no clouds; “cloud state” (00) and “pixel is adjacent to cloud” (0), (c) low or average aerosol quantity; “aerosol quantity” (01 or 10) in the 1km state QA of MOD09GA products (Ryu et al., 2014; Zhao and Running, 2010)

To compare field observation, high and low resolution satellite data, we used Landsat and Sentinel 2 data. Landsat has a 30m resolution and provide 16days data and Sentinel 2 has a 10m resolution and provide 10days data. We choose the data observed by Sentinel2 and Landsat with a cloud cover of less than 20%. We processed Sentinel 2 data using Sentinel Application Platform (SNAP) and Landsat using Matlab.

3 Results

3.1 Seasonal variation in 4S LED sensor

The performance of 4S LED sensor and Jaz hyper spectrometer well matched vegetation indices during transplanting to harvest ($y = 0.98x-0.07$, $R^2 = 0.98$, Bias = 0.016, RMSE = 0.05 for NDVI, $y = 0.94x-0.02$, $R^2 = 0.96$, Bias = 0.009, RMSE= 0.05 for EVI). NDVI and EVI values dropped after harvest suddenly (DOY 248). However, EVI showed different magnitude between 4S LED and Jaz after harvesting (4S: 0.2, Jaz: 0.1).

After DOY 140 NDVI and EVI increased. After harvest, DOY 209, EVI fell with a sharp drop. NDVI, on the other hand, gradually decreased but had a sudden drop after harvest (Figure 7).

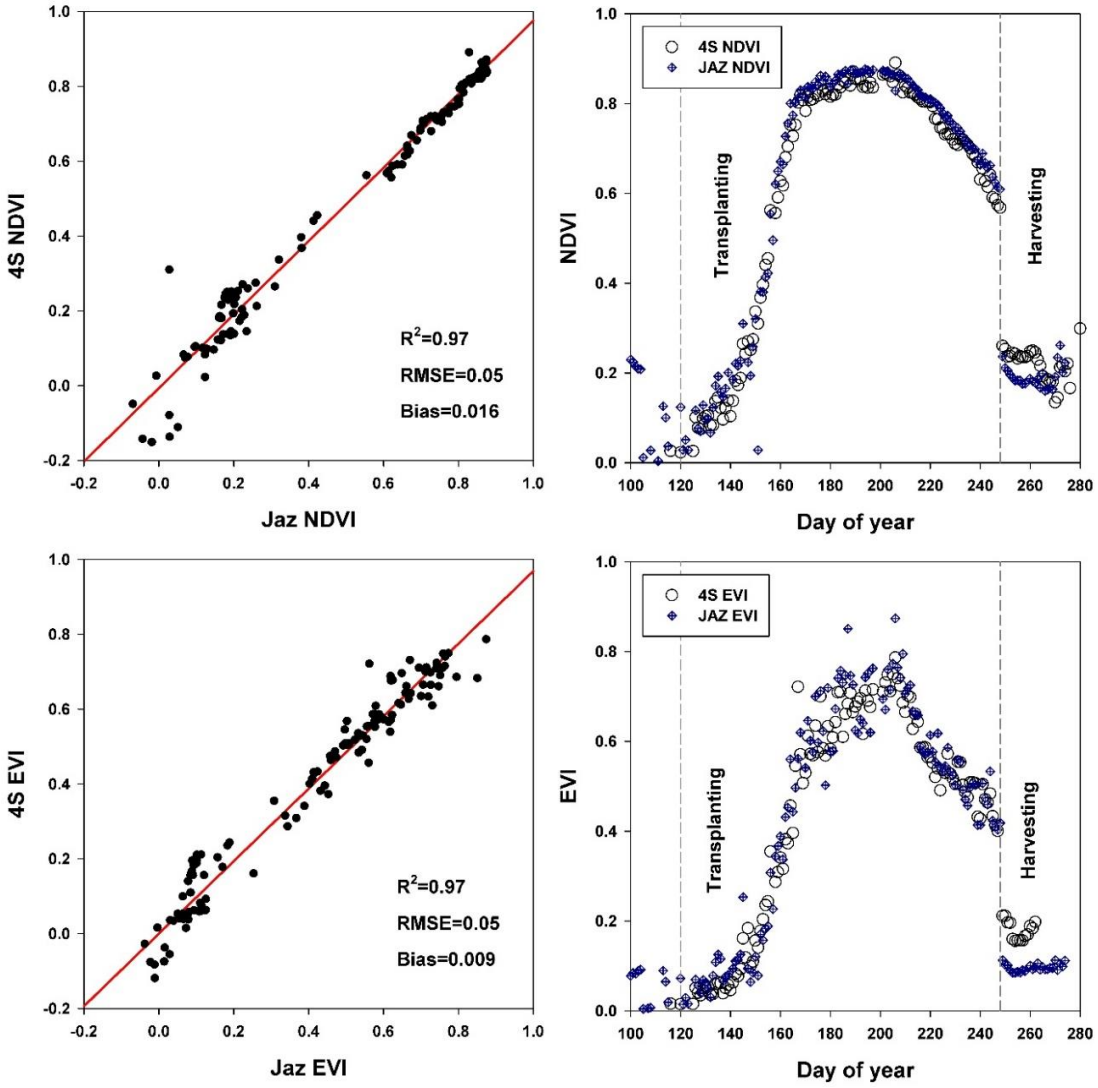

Figure 7) Comparison of NDVI and EVI observed using Jaz and LED. The performance of 4S LED sensor and Jaz hyper spectrometer well matched during transplanting to harvest.

When we compared fPAR from 4S and LAI2200, the magnitude and seasonal patterns were similar (R^2 = 0.99, Bias = 0.014, RMSE = 0.06). Observed 4S fPAR showed that the magnitude was kept constant after DOY 209 without a decreasing pattern. After harvest (DOY 248), 4S fPAR had some noise, whereas the fPAR observed with LAI2200 could not be estimated because the PAR observed below are larger than the PAR observed above (Figure 8).

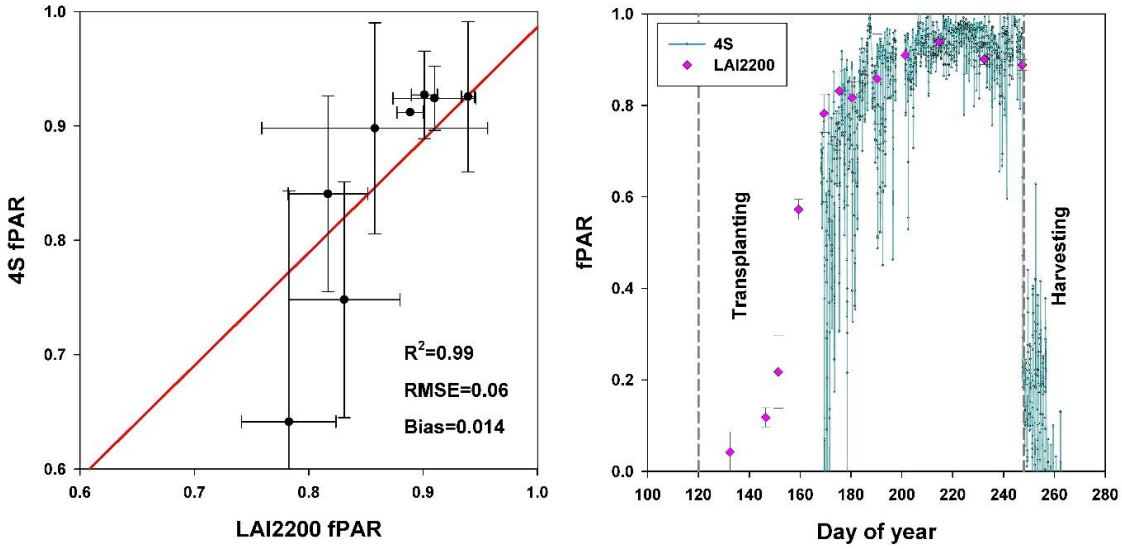

Figure 8) Comparison of fPAR observed using 4S and LAI2200. The yellow curve indicates 4S fPAR.

3.2 Seasonal variation in 4S camera sensor

We compared 4S LAI by using method of image histogram with LAI2200, harvest LAI, and harvest green LAI. The performance of 4S LAI is best matched to harvest green LAI during the period of transplanting to harvest ($y = 0.81x+0.5$, $R2 = 0.9$). When LAI increased or decreased, the 95% CI of 4S is relatively small, but when the LAI was 4 or more, the error range greatly increased. LAI gradually decreased, from the DOY 210, but LAI fluctuated more than when the leaf area increased (Figure 9).

After DOY 201, the Plant Area Index (PAI) quantified by LAI2200 shows an overestimation than harvest LAI, harvest green LAI and 4S LAI and in particular, the difference between harvest LAI with LAI2200 LAI was large.

The maximum value of harvest LAI was 6.58 at DOY 190, while the LAI estimated by 4S was 5.9 at DOY 209. After harvesting, the estimated LAI was zero.

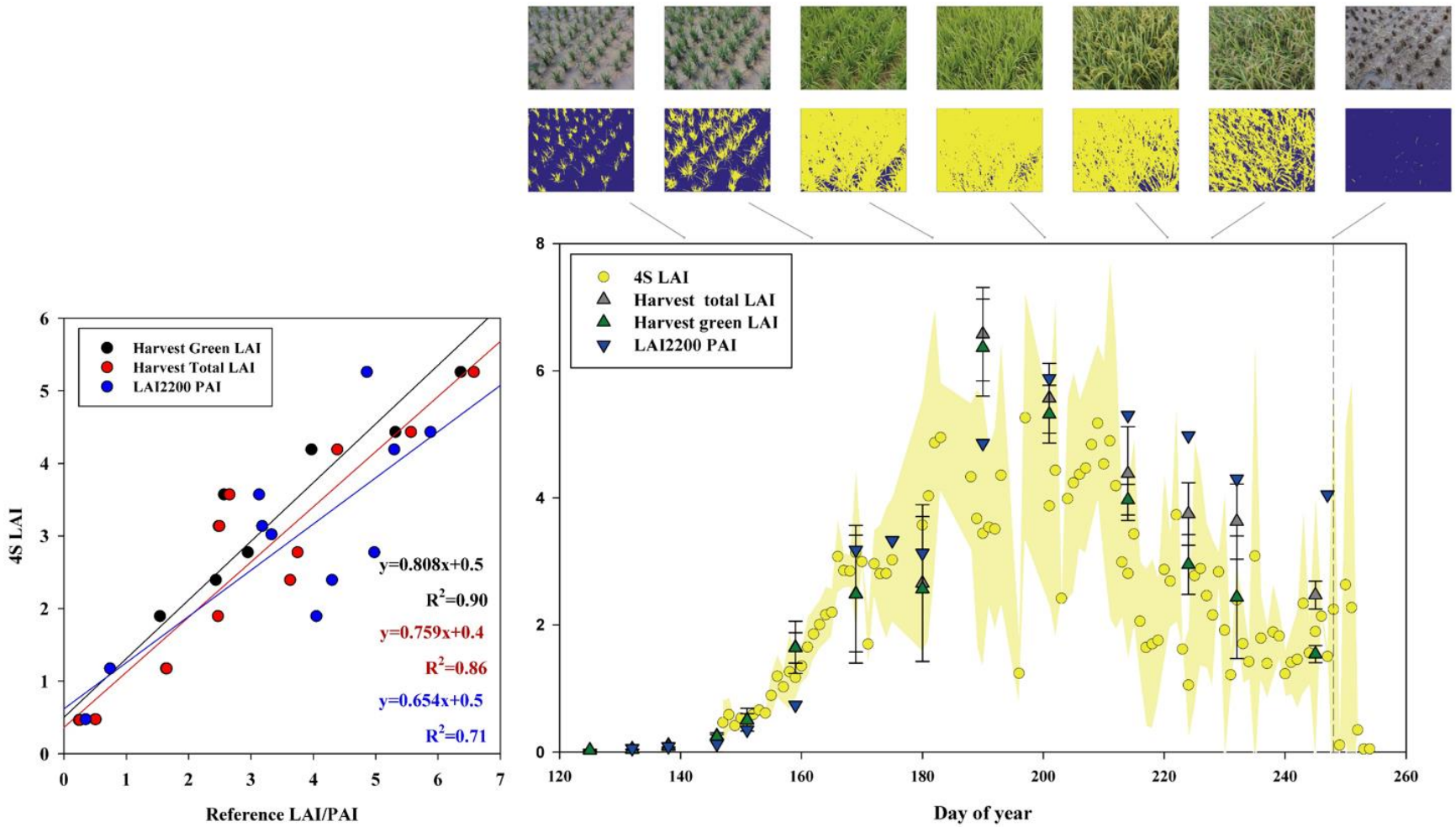

Figure 9) Comparison of LAI observed using 4S, harvest green LAI, harvest total LAI and LAI-2200 LAI. a) RGB photos from 4S. b) Images from 4S are selectively extracted from only the desired part

3.3 Comparison of NDVI obtained from 4S and satellites with different resolutions

Satellite and field observations are similar in magnitude and pattern to DOY 180 regardless of satellite resolution. After transplanting, we extracted NDVI from MODIS during DOY 120 to 155 and MODIS overestimated NDVI by 0.1 when compared to field observations. When the cloud-free data were obtained, Sentinel was able to get 6 values, and Landsat got 2 points during the growing season. More than 66% of all satellite observations were contaminated with clouds in the middle of the growing season (DOY 160 to 230) because of monsoon climate (Figure 10). After harvest, Sentinel2 (10m) well matched with field observations, but MODIS terra and aqua overestimated (250m).

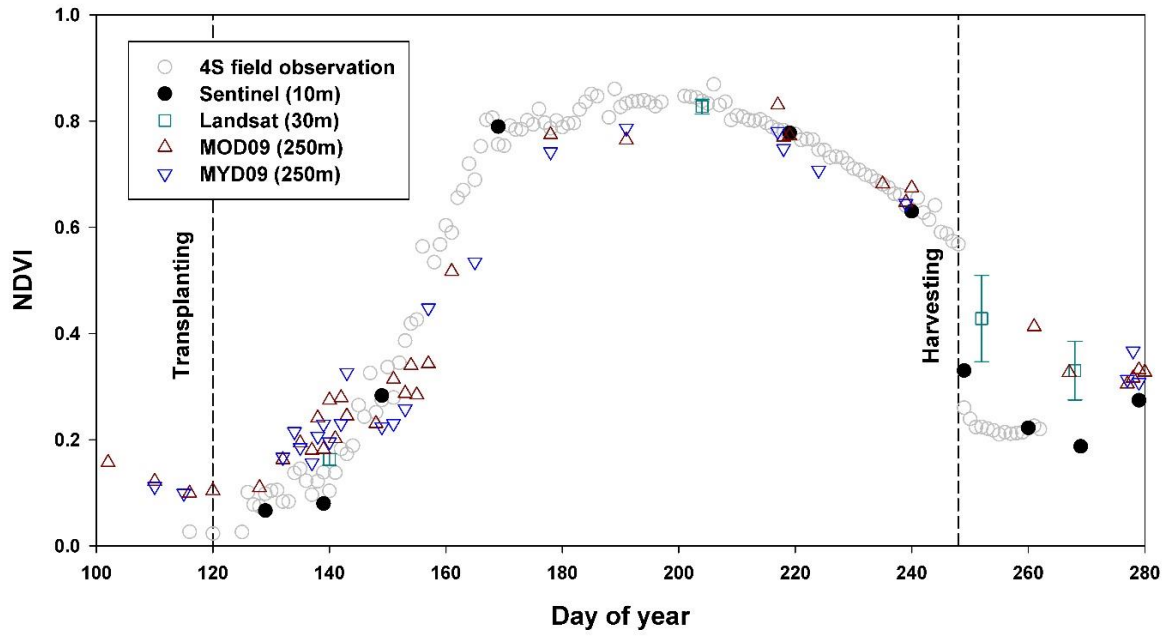

Figure 10) Comparison of NDVI observed using 4S and satellites with different resolutions.

4 Discussion

4.1 What are the advantages of 4S development?

4S is a combination of a camera and a LED spectrometer and is designed to automatically analyze data. By comparing with existing sensors such as Jaz hyper-spectrometer and LAI-2200 during the period of transplanting to harvest, 4S based vegetation indices, fPAR and LAI clearly showed reliable values. 4S was albe to track seasonal variation in vegetation indices (Figure7, EVI: R^2=0.95, NDVI: R^2=0.98). NDVI shows higher linearity with Jaz hyperspectrometer than EVI because EVI observed by 4S was ovrestimated compared to Jaz hyperspectrometer by 0.1 because of calibration problems for the blue band in LED sensors after harvest. Although we installed below LED late in under the canopy, the fPAR observed at 4S was similar to that observed with the LAI2200 (Figure8, fPAR: R^2=0.99). We calculate LAI using the histogram which was taken by images from 4S camera. As a results, LAI observed by 4S agreed with harvest green LAI (Figure9, LAI: R^2=0.95).

Although previous study tried to measure spectral reflectance of vegtation using LED, there is no research which has also measured PAR using LED (Jo et al., 2015; Ryu et al., 2010a; Ryu et al., 2014). We confirmed that combining red, green, and blue band from LEDs can show linear relationship with PAR sensor (Figure 4). By observing spectral reflectance and PAR simultaneously using LEDs, the number of installed sensors can be reduced and the labor requried to manage can be reduced. When we calculated the fPAR, we did not remove the reflectance from soil, water of vegetation, so the value is likely to be overestimated. Nevertheless, when fPAR was observed using 4S and LAI2200 in the same way, it was confirmed that there was no significant difference from LAI2200 (Figure 8).

Previous studies have tried to estimate LAI using hitogram from digital photography in the crop, however, studies that estimate LAI during the entire growing season are rare (Lee and

Lee, 2011; Liu and Pattey, 2010). The estimating LAI of crop land using a histogram has been done only during the early stages because it is easy to distinguish background such as water and soil from leaf in early stages. We confirmed that 4S can estimate LAI of rice continuously using the histogram obtained from digital photography (Figure 9). After vegetation reaches its reproductive stage, the size of rice becomes larger and the amount of the leaves increases making it hard to distinguish between background and leaf as the background becomes invisible. Therefore, using the histogram processed from image is challenged. We found that our method has the highest correlation with harvest green LAI, even though the threshold is selected empirically. Nevertheless, LAI estimation using a histogram, which is not an arbitary threshold designation as in the forest, is also needed for crop land (Hwang et al., 2016; Lang et al., 2010; Macfarlane, 2011).

4.2 What are the advantage of observing vegetation indices, fPAR and LAI independently?

There are efforts to continually estimate the vegetation indices, fPAR and LAI using the relationship between variables because it is difficult to measure each variable directly, however, we found that there are limitations. The limitation of estimating fPAR and LAI using vegetation indices is that the seasonal relationship is significantly different. NDVI and LAI decreased immediately after their peak, but fPAR remained constant (Figure 7, 8, 9). The reason why the seasonal pattern of each variable is different is that the influence of non-photosynthetic materials are large when the percentage of grain and yellow leaf are compared with variables (Figure 11). Previous studies have pointed out these problems. The relationship between NDVI and LAI observed in the field shows an exponential graph in which the slope of the graph is different for each phenophase (Vaesen et al., 2001). After the reproductive stage, fPAR remains constant even though NDVI decreases (Casanova et al., 1998; Rossini et al., 2010) as the formation of non-photosynthetic materials affect fPAR (Inoue et al., 2008; Viña and Gitelson, 2005).

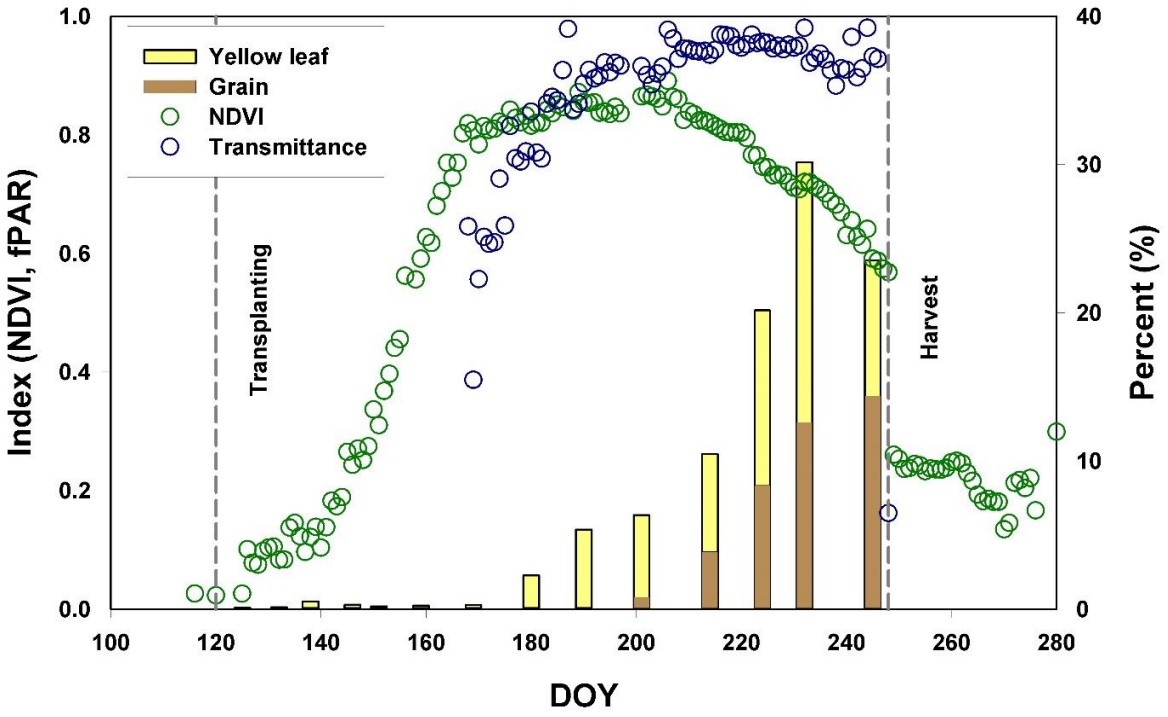

Figure 11) Comparison of NDVI and fPAR with percentage of grain and yellow leaf. The dash lines are transplanting and harvest day. As the grain begins to form, the fPAR remains constant while the NDVI decreases.

LAI derived from fPAR have a few drawbacks. First, the non-photosynthetic materials such as grains and yellow leaves affects transmittance. We found that PAI estimated by LAI2200 is overestimated compared to harvest LAI, harvest green LAI and 4S LAI (Figure 9). The LAI calculated using gap fraction was 1.5 higher than the LAI calculated by harvesting because it contains other materials besides the leaf. In the case of rice, the proportion of grain and yellow leaf was large, so 24% of the highest LAI was identified as non-photosynthetic materials. Second, according to Casanova et al. (1998), the extinction coefficient (K) differs depending on the phase of growth. Because the angle of the leaves changes from erectophile to planophile (K=0.35 during the vegetative stage, K=0.47 during the reproductive and K=0.62 during the reproductive period). Therefore, effective LAI, which is estimated by fPAR, can be

overestimated compared to harvest LAI after the leaf starts turning yellow and grains begin to increase (Figure 11).

Previous studies estimated fPAR by using NDVI directly or by making similar formulas using specific wavelength (Asrar et al., 1984; Hatfield et al., 1984; Inoue et al., 2008; Lind and Fensholt, 1999). When we compared seasonal patterns of fPAR, however, we found that it remains constant after the reproductive period unlike NDVI (Figure 11). Therefore, there is an error in estimating the fPAR using NDVI with the same formula during the growing season (Figure 7, 8). In our observation, we found that estimation of the diurnal pattern of fPAR using NDVI also had limitation (Figure 12). Vegetation indices are constant over the changing Solar Zenith Angle (SZA). On the other hand, fPAR has diurnal pattern according to SZA especially when the LAI is small and the leaf angle is low because if the sun located vertical, the light is easy to be transmitted light. The observed fPAR remains constant in cloud day because the light condition is diffusing on a cloudy day (Figure 12).

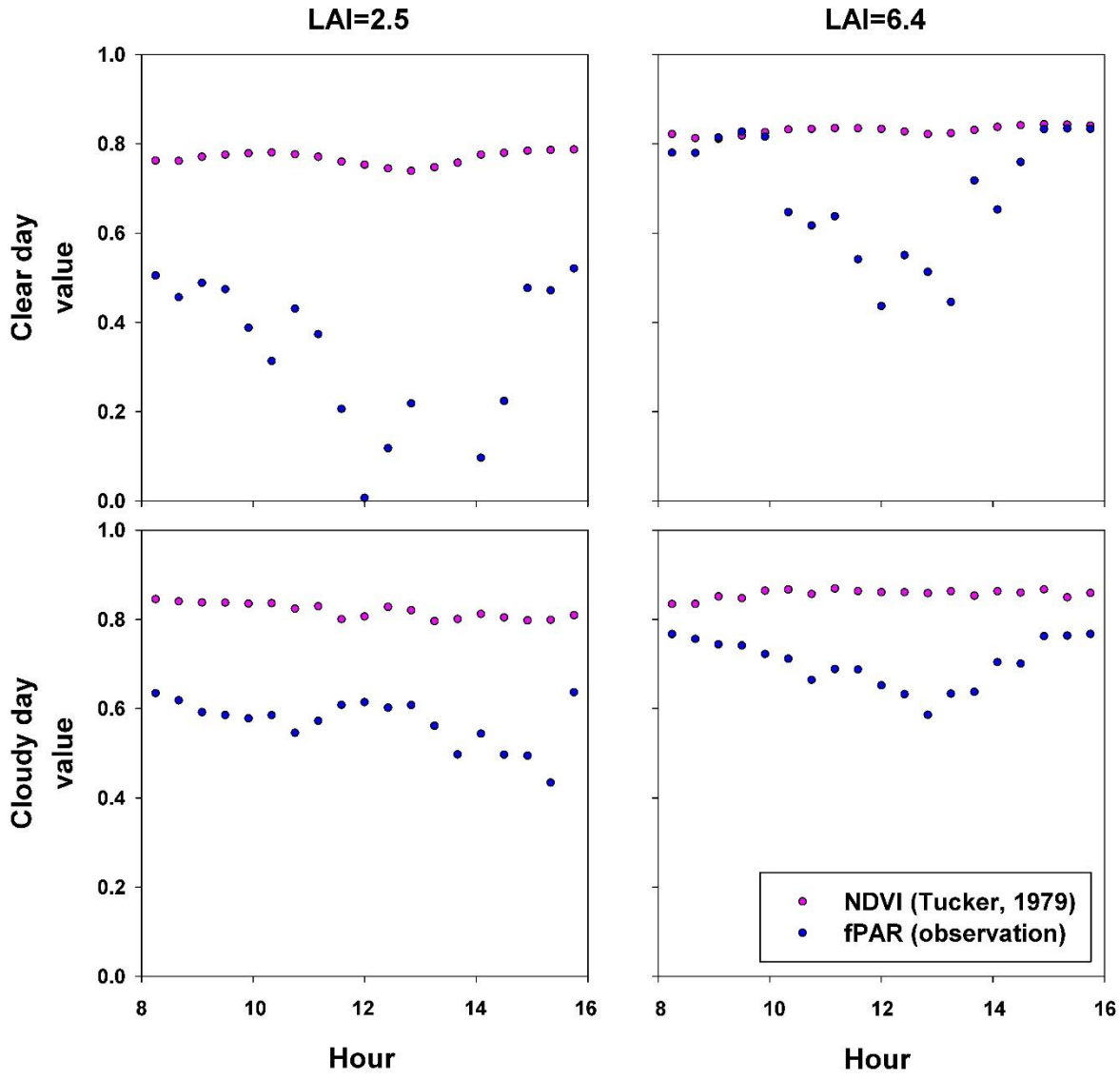

Figure 12) Comparison of diurnal pattern of indices made to estimate fPAR, observed fPAR and NDVI on clear day and cloud day.

4.3 What are the advantages of continuous observation compared to different sensors?

The data collected using 4S has a significantly smaller data gap than the satellite data; 4S data gap (1- Observed days/Growing season days x 100) is 4.68%, Sentinel gap (1- Observed days/Growing season days x 100) is 95.36% and Landsat gap is 66%. In case of MODIS, data gap of aqua is 85% and terra is 80% (Figure 10). Combining MODIS Terra and Auqa show that percent of data gap is 77%. Combined observation can reduce data gap that results from atmospheric condition. A previous study reported that over 80% of MODIS data in the monsoon climate was affected by clouds and combination of multiple satellite sensors is one possible solution to avoid cloud contamination (Motohka et al., 2009). However, even though we combine data from two satellite sensors, there are overlapping days and it is difficult to avoid the influence of clouds over summer moonson climate. 4S could observe changing rice paddy because the near surface sensor is less affected by the weather condition.

By comparing field observations with the satellite observations, we found that low temporal resolution and high spatial resolution satellites show similar magnitude and pattern with field observation. Before and after transplanting, all satellites data were similar to field observations regardless of resolution. NDVI observed by MODIS Terra, Aqua and Landsat shows overestimate than field observation after harvest. On the other hand, Sentinel2 with a resolution of 10m shows similar value to 4S (Figure 10). The large spatial resolution of data is the major limitation for monitoring vegetation, especially crop management (Inoue, 2003). The satellite products show similar magnitude with 4S due to large proportion of water in the rice paddy during the early stage (Figure 13). The distribution of the histogram shows that the average number of pixels is highest and is homogeneously distributed around the average value, near the transplanting day. However, during harvesting, the standard deviations (0.11) are larger than transplanting days (0.095) and scattered rather than converging to mean values because the patch area of the managed rice is small and the farmers harvest at different times. We was

able to clearly see the images observed at Sentinel2 (Figure 13). Therefore, it is difficult to estimate the harvest day at a site scale using low spatial resolution satellite data because of the large spatial resolution that covers heterogeneous regions.

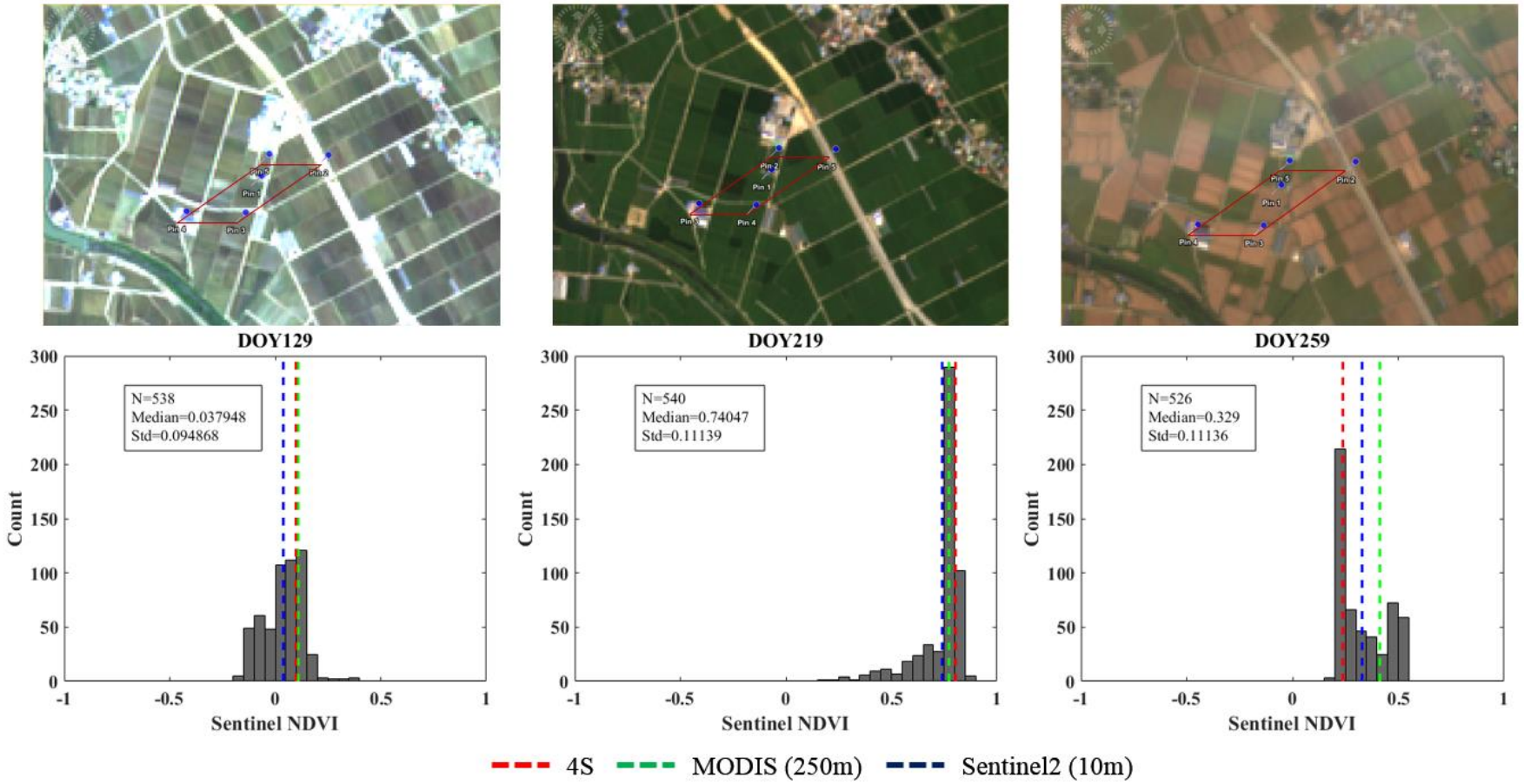

Figure 13) Statistical properties of Sentinel NDVI values. More than 500 Sentinel2 pixels within one 250m MODIS pixel that include the rice paddy tower. The red line indicate boundary of MODIS 250m and dash line is averaged value in each DOY.

5 Conclusion

The components of 4S are already well know, however, by melding them together into one, we present an novel system that can help us the complicated biophysical relationships in the ecosystem. The 4S system reliably measured vegetation indices and fPAR and estimated reliable LAI value when compared to Jaz hyper spectrometer, LAI2200 and harvesting green LAI. We obtain vegetation indices, fPAR and LAI independently and continuously and then found that the relationship of these variables changed after reproductive stage because of grain and yellow leaf. In additional, using vegetation index to estimate fPAR has limitation because the spectral reflectance could not capture diurnal pattern. When we compared with satellite data, which has different resolutions, 4S system showed more accurate NDVI due to the fine spatial and temporal resolution compared to satellite data in a heterogeneous and cloudy region. We expect that the novel system can make a valuable contribution to ecological observations.

6 Reference

Asrar, G., Fuchs, M., Kanemasu, E. and Hatfield, J., 1984. Estimating absorbed photosynthetic radiation and leaf area index from spectral reflectance in wheat. Agronomy journal, 76(2): 300-306.

Baldocchi, D.D., Matt, D.R., Hutchison, B.A. and McMillen, R.T., 1984. Solar radiation within an oak—Hickory forest: An evaluation of the extinction coefficients for several radiation components during fully-leafed and leafless periods. Agricultural and Forest Meteorology, 32(3-4): 307-322.

Baldocchi, D.D., Wilson, K.B. and Gu, L., 2002. How the environment, canopy structure and canopy physiological functioning influence carbon, water and energy fluxes of a temperate broad-leaved deciduous forest-an assessment with the biophysical model CANOAK. Tree Physiology, 22(15): 1065-1077.

Bauer, J., Siegmann, B., Jarmer, T. and Aschenbruck, N., 2014. On the potential of Wireless Sensor Networks for the in-field assessment of bio-physical crop parameters, Local Computer Networks Workshops (LCN Workshops), 2014 IEEE 39th Conference on. IEEE, pp. 523-530.

Begue, A., 1991. Estimation de la production primaire en zone sahélienne à partir de données radiométriques. Cas d'un couvert discontinu: le mil.

Campbell, G., 1990. Derivation of an angle density function for canopies with ellipsoidal leaf angle distributions. Agricultural and forest meteorology, 49(3): 173-176.

Casanova, D., Epema, G. and Goudriaan, J., 1998. Monitoring rice reflectance at field level for estimating biomass and LAI. Field Crops Research, 55(1): 83-92.

Ferrández-Pastor, F., García-Chamizo, J., Nieto-Hidalgo, M., Mora-Pascual, J. and Mora-Martínez, J., 2016. Developing Ubiquitous Sensor Network Platform Using Internet of Things: Application in Precision Agriculture. Sensors, 16(8): 1141.

Garrity, S.R., Vierling, L.A. and Bickford, K., 2010. A simple filtered photodiode instrument for continuous measurement of narrowband NDVI and PRI over vegetated canopies. Agricultural and Forest Meteorology, 150(3): 489-496.

Goel, N.S. and Strebel, D.E., 1984. Simple beta distribution representation of leaf orientation in vegetation canopies. Agronomy Journal, 76(5): 800-802.

Gressler, E., Jochner, S., Capdevielle-Vargas, R.M., Morellato, L.P.C. and Menzel, A., 2015. Vertical variation in autumn leaf phenology of Fagus sylvatica L. in southern Germany. Agricultural and Forest Meteorology, 201: 176-186.

Hatfield, J., Asrar, G. and Kanemasu, E., 1984. Intercepted photosynthetically active radiation estimated by spectral reflectance. Remote Sensing of Environment, 14(1-3): 65-75.

Hilker, T., Coops, N.C., Nesic, Z., Wulder, M.A. and Black, A.T., 2007. Instrumentation and approach for unattended year round tower based measurements of spectral reflectance. Computers and Electronics in Agriculture, 56(1): 72-84.

Huete, A. et al., 2002. Overview of the radiometric and biophysical performance of the MODIS vegetation indices. Remote sensing of environment, 83(1): 195-213.

Hwang, Y. et al., 2016. Correction for light scattering combined with sub-pixel classification improves estimation of gap fraction from digital cover photography. Agricultural and Forest Meteorology, 222: 32-44.

Inoue, Y., 2003. > Synergy of Remote Sensing and Modeling for Estimating Ecophysiological Processes in Plant Production. Plant Production Science, 6(1): 3-16.

Inoue, Y., Peñuelas, J., Miyata, A. and Mano, M., 2008. Normalized difference spectral indices for estimating photosynthetic efficiency and capacity at a canopy scale derived from hyperspectral and CO 2 flux measurements in rice. Remote Sensing of Environment, 112(1): 156-172.

Jenkins, J. et al., 2007. Refining light-use efficiency calculations for a deciduous forest canopy using simultaneous tower-based carbon flux and radiometric measurements. Agricultural and Forest Meteorology, 143(1): 64-79.

Jiang, Z., Huete, A.R., Didan, K. and Miura, T., 2008. Development of a two-band enhanced vegetation index without a blue band. Remote Sensing of Environment, 112(10): 3833-3845.

Jo, S., Eom, I.-Y., Ko, J. and Kang, S., 2015. Development of a light-emitting-diode-based bidirectional active remote-sensing system for monitoring crop growth. International Journal of Remote Sensing, 36(5): 1424-1438.

Lang, M., Kuusk, A., Mõttus, M., Rautiainen, M. and Nilson, T., 2010. Canopy gap fraction estimation from digital hemispherical images using sky radiance models and a linear conversion method. Agricultural and Forest Meteorology, 150(1): 20-29.

Lee, K.-J. and Lee, B.-W., 2011. Estimating canopy cover from color digital camera image of rice field. Journal of Crop Science and Biotechnology, 14(2): 151-155.

Leuning, R., Kelliher, F., Pury, D.d. and SCHULZE, E.D., 1995. Leaf nitrogen, photosynthesis, conductance and transpiration: scaling from leaves to canopies. Plant, cell & environment, 18(10): 1183-1200.

Liao, M.-S. et al., 2017. On precisely relating the growth of Phalaenopsis leaves to greenhouse environmental factors by using an IoT-based monitoring system. Computers and Electronics in Agriculture, 136: 125-139.

Lind, M. and Fensholt, R., 1999. The spatio-temporal relationship between rainfall and vegetation development in Burkina Faso. Geografisk Tidsskrift: 43-56.

Liu, J. and Pattey, E., 2010. Retrieval of leaf area index from top-of-canopy digital photography over agricultural crops. Agricultural and Forest Meteorology, 150(11): 1485-1490.

Macfarlane, C., 2011. Classification method of mixed pixels does not affect canopy metrics from digital images of forest overstorey. Agricultural and Forest Meteorology, 151(7): 833-840.

Mell, P. and Grance, T., 2011. The NIST definition of cloud computing.

Miorandi, D., Sicari, S., De Pellegrini, F. and Chlamtac, I., 2012. Internet of things: Vision, applications and research challenges. Ad Hoc Networks, 10(7): 1497-1516.

Monteith, J.L., 1965. Evaporation and environment, Symp. Soc. Exp. Biol, pp. 4.

Monteith, J.L., 1976. Vegetation and the atmosphere. Volume 2. Case studies. Academic Press.

Motohka, T., Nasahara, K., Miyata, A., Mano, M. and Tsuchida, S., 2009. Evaluation of optical satellite remote sensing for rice paddy phenology in monsoon Asia using a continuous in situ dataset. International Journal of Remote Sensing, 30(17): 4343-4357.

Myneni, R., Asrar, G. and Kanemasu, E., 1987. Light scattering in plant canopies: The method of successive orders of scattering approximations (SOSA). Agricultural and forest meteorology, 39(1): 1-12.

Myneni, R.B., Keeling, C., Tucker, C.J., Asrar, G. and Nemani, R.R., 1997a. Increased plant growth in the northern high latitudes from 1981 to 1991. Nature, 386(6626): 698.

Myneni, R.B., Ramakrishna, R., Nemani, R. and Running, S.W., 1997b. Estimation of global leaf area index and absorbed PAR using radiative transfer models. IEEE Transactions on Geoscience and remote sensing, 35(6): 1380-1393.

Nagai, S. et al., 2014. Relationship between spatio-temporal characteristics of leaf-fall phenology and seasonal variations in near surface- and satellite-observed vegetation indices in a cool-temperate deciduous broad-leaved forest in Japan. International Journal of Remote Sensing, 35(10): 3520-3536.

Qu, Y., Zhu, Y., Han, W., Wang, J. and Ma, M., 2014. Crop leaf area index observations with a wireless sensor network and its potential for validating remote sensing products. IEEE Journal of Selected Topics in Applied Earth Observations and Remote Sensing, 7(2): 431-444.

Richardson, A.D., Klosterman, S. and Toomey, M., 2013. Near-Surface Sensor-Derived Phenology. 413-430.

Rossini, M. et al., 2010. High resolution field spectroscopy measurements for estimating gross ecosystem production in a rice field. Agricultural and Forest Meteorology, 150(9): 1283-1296.

Ryu, Y. et al., 2010a. Testing the performance of a novel spectral reflectance sensor, built with

light emitting diodes (LEDs), to monitor ecosystem metabolism, structure and function. Agricultural and Forest Meteorology, 150(12): 1597-1606.

Ryu, Y., Lee, G., Jeon, S., Song, Y. and Kimm, H., 2014. Monitoring multi-layer canopy spring phenology of temperate deciduous and evergreen forests using low-cost spectral sensors. Remote Sensing of Environment, 149: 227-238.

Ryu, Y. et al., 2010b. On the correct estimation of effective leaf area index: Does it reveal information on clumping effects? Agricultural and Forest Meteorology, 150(3): 463-472.

Ryu, Y. et al., 2012. Continuous observation of tree leaf area index at ecosystem scale using upward-pointing digital cameras. Remote Sensing of Environment, 126: 116-125.

Sellers, P. et al., 1997. Modeling the exchanges of energy, water, and carbon between continents and the atmosphere. Science, 275(5299): 502-509.

Tucker, C.J., 1979. Red and photographic infrared linear combinations for monitoring vegetation. Remote sensing of Environment, 8(2): 127-150.

Vaesen, K., Gilliams, S., Nackaerts, K. and Coppin, P., 2001. Ground-measured spectral signatures as indicators of ground cover and leaf area index: the case of paddy rice. Field Crops Research, 69(1): 13-25.

Viña, A. and Gitelson, A.A., 2005. New developments in the remote estimation of the fraction of absorbed photosynthetically active radiation in crops. Geophysical Research Letters, 32(17).

Yin, G. et al., 2017. Derivation of temporally continuous LAI reference maps through combining the LAINet observation system with CACAO. Agricultural and Forest Meteorology, 233: 209-221.

Zhao, M. and Running, S.W., 2010. Drought-induced reduction in global terrestrial net primary production from 2000 through 2009. science, 329(5994): 940-943.

Zhen, J., Tripler, E., Peng, X. and Lazarovitch, N., 2017. A wireless device for continuous frond elongation measurement. Computers and Electronics in Agriculture, 140: 1-7.

Abstract (Korean)

식생 지수, 광합성유효복사량의 흡수율 그리고 엽면적 지수를 지속적으로 관측하는 것은 생물권과 대기권의 상호작용을 이해를 증진 시켰다. 그럼에도 불구하고, 식생 지수, 광합성유효복사량의 흡수율 그리고 엽면적 지수를 동시에 지속적으로 관측하는 것은 여전히 부족하다. 최근 발전된 기술은 저렴한 센서 간의 결합이 가능하게 함으로써 생태계의 구조와 기능을 보다 현명하게 관측할 수 있는 기회를 제공한다. 본 연구에서, 우리는 Smart Surface Sensing System (4S)라는 스스로 데이터를 수집, 전송 분석하고 실시간으로 인터넷을 통해 확인 할 수 있는 시스템을 개발 하였다. 이 시스템은 소형 컴퓨터, 소형 제어기, LED를 이용한 다중 분광계, 소형 카메라, 그리고 인터넷 모듈이 결합되어 있다. 우리는 연구실 내에서 시스템에 대한 검증과 보정을 하고 실제로 농경지에서 normalized difference vegetation index (NDVI), enhanced vegetation index (EVI), 광합성유효복사의 흡수율 (fPAR), 그리고 엽면적 지수 (LAI)를 지속적으로 생장 기간 동안 관측하였다. 4S로 관측한 NDVI와 EVI는 초 분광계에서 관측한 것과 비교 했을 때 선형적인 관계를 나타냈다. (R^2 = 0.98; NDVI, R^2 = 0.96; EVI). 4S로 관측한 fPAR와 LAI는 LAI2200와 직접 관측한 값과 비교했을 때, 양적으로나 시계절적으로 일치하는 것을 확인 하였다. 우리는 동시에 식생 지수 fPAR 그리고 LAI를 독립적으로 그리고 지속적으로 관측함으로써 벼의 생식 단계 이후의 fPAR는 일정하게 값이 유지되지만 NDVI와 LAI는 정점 이후의 지속적으로 감소하는 것을 확인하였는데, 이는 광합성에 사용되지 않는 인자들, 벼나

노란색 잎들이 생성되기 때문이다. 게다가, 식생 지수를 이용하여 fPAR를 추정할 때 한계가 있음을 확인하였다. 식생 지수는 뚜렷한 일 주기 변화를 보이지 않았으나, fPAR는 하늘 상태나 빛이 투과할 수 있는 정도에 따라 일 주기의 변화가 극심한 것을 확인하였다. 우리는 4S가 다양한 공간과 시간적 조건에서 생태학적 센서 네트워크를 확장하는데 도움이 될 것이라 믿는다.

주요 단어: 엽면적 지수, 식생 지수, 광합성유효복사량의 흡수율, 근접표면센서, 원격 탐사

학번: 2015-23120